

# Numerical and experimental investigation on static electric charge model at stable cone-jet region

Ali Reza Hashemi,<sup>1</sup> Ahmad Reza Pishevar,<sup>1,a)</sup> Afsaneh Valipouri,<sup>2</sup> and Emilian I. Părău<sup>3</sup>

<sup>1</sup>Department of Mechanical Engineering, Isfahan University of Technology, Isfahan 84156-83111, Iran

<sup>2</sup>Department of Textile Engineering, Isfahan University of Technology, Isfahan 84156-83111, Iran

<sup>3</sup>School of Mathematics, University of East Anglia, Norwich NR4 7TJ, United Kingdom

In a typical electro-spinning process, the steady stretching process of the jet beyond the Taylor cone has a significant effect on the dimensions of resulting nanofibers. Also, it sets up the conditions for the onset of the bending instability. The focus of this work is the modeling and simulation of the initial stable jet phase seen during the electro-spinning process. The perturbation method was applied to solve hydrodynamic equations, and the electrostatic equation was solved by a boundary integral method. These equations were coupled with the stress boundary conditions derived appropriate at the fluid-fluid interface. Perturbation equations were discretized by the second-order finite difference method, and the Newton method was implemented to solve the discretized nonlinear system. Also, the boundary element method was utilized to solve the electrostatic equation. In the theoretical study, the fluid is described as a leaky dielectric with charges only on the jet surface in dielectric air. In this study, electric charges were modeled as static. Comparison of numerical and experimental results shows that at low flow rates and high electric field, good agreement was achieved because of the superior importance of the charge transport by conduction rather than convection and charge concentration. In addition, the effect of unevenness of the electric field around the nozzle tip was experimentally studied through plate-plate geometry as well as point-plate geometry.

## I. INTRODUCTION

Electro-spinning is the most popular strategy for producing ultrafine fibers by electrically charging a droplet of polymer liquid. The fiber diameters could be as small as a few nanometers if electro-spinning takes place under appropriate spinning conditions. The remarkable characteristics of the nanofibers, such as high surface areas and possibilities for efficient surface functionalization, make them a promising candidate in technical areas such as filters, textiles, and nanofiber reinforcement as well as in medicinal areas such as tissue engineering, wound healing, and drug delivery.<sup>1</sup>

In electro-spinning, the tensile force is generated by the interaction of an applied electric field with the electrical charge carried by jet. Once a threshold voltage is applied to the polymer solution of the Newtonian or non-Newtonian fluid, a critical value is obtained at which the electrostatic forces overcome the surface tension and a straight jet is formed, as a consequence of electrical forces, from a conical protrusion, often called a Taylor cone, on the surface of a pendant drop of solution. This jet travels for a few centimeters in a straight line toward the collector, and at the end of this steady stretching process, the jet follows a bending, whipping, spiraling, and looping path in three dimensions. The jet in each loop is grown longer and thinner as the loop diameter and circumference are increased.<sup>2</sup> The steady stretching process is important in that it not only contributes to the thinning directly but also sets up the

conditions for the onset of the bending instability. However, bending instabilities in electro-spun jets play the principal role in elongation and thinning electro-spun jet.

With the renewed interest in nanotechnology in a recent decade, many studies have been focused on the production of nanofibers, whilst some theoretical studies have been performed. There are several models that have been proposed to explain the initial development of electro-spun jets by Hartman *et al.*,<sup>3</sup> Spivak *et al.*,<sup>4</sup> Hohman *et al.*,<sup>5,6</sup> Shin *et al.*,<sup>7</sup> Feng,<sup>2,8</sup> Yan *et al.*,<sup>9</sup> Carroll and Joo<sup>10,11</sup> as well as by Reneker and Yarin<sup>12</sup> and Higuera.<sup>13-15</sup> Recently, some studies have been developed to predict nanofiber properties. Some of this research involved using available models,<sup>2,12</sup> and some others have statistically predicted nanofiber properties using experimental data.<sup>16-23</sup>

In this paper, we considered only the steady stretching process of the electro-spun jet. We numerically analyzed the behavior of an incompressible Newtonian jet under the uniform external electric field. The fluid was described as a leaky dielectric with charges only on the jet surface. Electrohydrodynamic (EHD) equations were derived using the perturbation method. The electrostatic equation which is the Laplace equation was solved using the boundary integral technique, as conducted by Lac and Homsy.<sup>24</sup> With a leaky dielectric model, the low conductivity fluid causes the formation of a thin layer of electric charges on the interface. The dynamics of electric charge transport at the fluid-fluid interface is described by the charge conservation equation (see Ref.<sup>25</sup>). The main essential transport mechanisms in this equation are the charge

<sup>a)</sup> Author to whom correspondence should be addressed: apishe@cc.iut.ac.ir

accumulation at the interface due to conduction and the jump in the conventional charge current in the bulk across the interface; surface convection of the interfacial charges; effect of stretching of the interface; and surface conduction. In the present study, due to low flow rates and high voltages, the charge convection term can be eliminated from the governing equation. Moreover, by assuming the instantaneous migration of electric charges toward the interface, concentration change due to the surface dilation in the transport of electric charges is negligible and the electric current across the interface will become con-

tinuous. Hence, the surface charge conservation equation is reduced to a boundary condition at the interface. This model which was well adapted for the leaky dielectric systems is called the static model for surface charges.

The geometry of the nozzle plays a major role in the applied electric field. Hohman *et al.*<sup>6</sup> indicated that the conductivity and the length of the nozzle protrude from the top capacitor plate cause a fringe field. Near this nozzle, the local field will be higher than the applied electric field between the two electrodes. Feng<sup>2</sup> stated that the effective parameters on the electric charges at the nozzle have depended on the nozzle geometry and the applied electric field; however, these facts have not been considered in the numerical models. Carroll and Joo<sup>10</sup> neglected the fringe fields around the spinneret. They believed that the electro-spinning setup which they used is slightly different from that used by Hohman *et al.*<sup>6</sup> in their setup, the needle is directly connected to the high voltage source without using a capacitor plate. Also, applied electric field intensities were much smaller than those examined by Hohman *et al.*<sup>6</sup> As well as Higuera<sup>14,15</sup> estimated the geometry of the nozzle as a conic metal tube which logarithmically changes the electric voltage between the two electrodes. The proposed numerical method for solving the

governing electrical equation in this study is capable of mimicking the effect of the nozzle in the uniform applied electric field without considering its geometry; subsequently, the resulted irregularity around the nozzle will be automatically compensated.

In addition, the effect of unevenness of the electric field around the nozzle tip was experimentally studied through plate-plate geometry as well as point-plate geometry. It was observed that the connection of the high voltage source to the nozzle will result in more irregularity in the electric field around the nozzle. This irregularity causes the deviation of the central axis of the jet from the straight path and elongates the jet in a shorter distance from the nozzle at low applied electric field. Current numerical results were compared to numerical and experimental results of previous studies for validation.

## II. GOVERNING EQUATIONS

The equation of continuity and momentum was applied to an incompressible Newtonian fluid, as

$$\nabla \cdot \mathbf{u} = 0, \quad (1)$$

$$\rho \frac{\partial \mathbf{u}}{\partial t} + (\mathbf{u} \cdot \nabla) \mathbf{u} = -\nabla p + \nabla \cdot \boldsymbol{\tau} + \rho \mathbf{g}, \quad (2)$$

where  $\mathbf{u}$  is the velocity,  $\rho$  is the density,  $p$  is the pressure,

hydrodynamic ( $\boldsymbol{\tau}^H$ ) and electric ( $\boldsymbol{\tau}^E$ ) components, and  $\mathbf{g}$  is the gravitational acceleration vector. For a leaky dielectric fluid, the electric force only applies to the fluid-fluid interface. Hence, the electric force will be a boundary term and the induced current will be formed only by the application of boundary conditions on the interface.<sup>26</sup> Saville<sup>25</sup> has expressed the jump condition of normal and tangential Maxwell electric stresses at the interface as presented in the following equations:

$$\mathbf{n} \cdot \boldsymbol{\tau}^E \cdot \mathbf{n}^T = \frac{\epsilon_0}{2} \epsilon (\mathbf{E} \cdot \mathbf{n})^2 - (\mathbf{E} \cdot \mathbf{t})^2, \quad (3)$$

$$\mathbf{t} \cdot \boldsymbol{\tau}^E \cdot \mathbf{n}^T = q^s (\mathbf{E} \cdot \mathbf{t}). \quad (4)$$

In these equations,  $\llbracket \cdot \rrbracket$  denotes the jump, *outside - inside*, of  $(\cdot)$  across the interface,  $\epsilon_0 \epsilon$  indicates the electric permittivity of the fluid,  $q^s$  is the electric charge surface density, and  $\mathbf{n}$  and  $\mathbf{t}$  are the unit normal and the tangential vectors to the free surface, respectively. In this study, electric charges were modeled as static and the electric charge density was obtained explicitly from the equation  $q^s = \epsilon_0 \epsilon \mathbf{E} \cdot \mathbf{n}$ .<sup>24,25</sup> Across the jet interface,  $\mathbf{E} \cdot \mathbf{t}$  is continuous, but  $\mathbf{E} \cdot \mathbf{n}$  undergoes a discontinuity due to the difference in physical properties of the two fluids.<sup>24</sup> In order to consider electric stresses in the momentum equation, the jump condition was applied across the interface. Additionally, surface tension results in pressure discontinuity across the interface. The pressure jump on the interface is directly proportional to the average of the surface local curvature and causes a difference in pressure between the inside and outside of the jet. With considering these two effects, the jump condition in normal stresses can be calculated as in the following equation:<sup>27</sup>

$$\llbracket \mathbf{n} \cdot (p \mathbf{I} - \boldsymbol{\tau}^T) \cdot \mathbf{n}^T \rrbracket = \frac{\gamma \kappa}{0}, \quad (5)$$

where  $\gamma$  is the surface tension,  $\kappa$  is the surface curvature, and  $\mathbf{I}$  is the unit tensor. The problem dimensionless parameters were listed in Table I, where  $U$  is the velocity of the jet at the nozzle outlet,  $a$  is the radius of the nozzle,  $R$  is the jet local radius,  $X$  is the jet axis coordinate, and  $E_{n,t}$  are the normal and the tangential electrical components on the interface. The dimensionless numbers in this study include Weber, Reynolds, Froude, Beta, electric permittivity ratio, and conductivity ratio as listed in Table II, where  $\mu$  is the dynamic viscosity, the magnitude of the external electric field is  $E_0$ , and  $\epsilon_0 \epsilon_o$  is the electric permittivity of the external fluid. In this study, the applied external electric field is uniform and its magnitude can be obtained by dividing the potential difference ( $\Delta\psi$ ) by the spinning distance ( $d$ ).

The basis used for solving the governing equations for an electrified jet is the perturbation theory proposed by Părău *et al.*,<sup>28</sup> who used this methodology to simulate the behavior

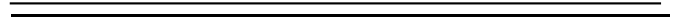
TABLE I. Dimensionless parameters.

$u$	$\frac{u}{U}$	$\frac{R}{a}$	$\frac{X}{a}$	$\frac{t}{a}$	$\frac{p}{\rho U^2}$	$\frac{q^s}{\epsilon_0 \epsilon_o}$	$\frac{E_{n,t}}{E_0}$
	$= U$	$R = \frac{R}{a}$	$X = \frac{X}{a}$	$t = \frac{t}{a}$	$\tilde{p} = \frac{p}{\rho U^2}$	$\tilde{q} = \frac{q^s}{\epsilon_0 \epsilon_o}$	$E_{n,t} = \frac{E_{n,t}}{E_0}$

TABLE II. Dimensionless numbers.

$We = \frac{\rho U^2 a}{\gamma}$	$Re = \frac{\rho U a}{\mu}$	$Fr = \frac{U^2}{ag}$	$\beta = \frac{\epsilon_0 \epsilon_n E^2}{\rho U^2}$	$\epsilon_{io} = \frac{\epsilon_i}{\epsilon_o}$	$\sigma_{oi} = \frac{\sigma_o}{\sigma_i}$
----------------------------------	-----------------------------	-----------------------	--	---	---

$\mathbf{T}$  is the deviatoric stress tensor which is composed of two



of a bent jet in the prilling process. They expand the velocity components, pressure, radius, and position components of the jet trajectory in asymptotic series by assuming that the jet is a long, slender object. They then substitute these expansions in continuity and momentum equations, as well as

boundary conditions, and after a few manipulations obtained the governing equations on the jet behavior. Certain assumptions have been considered such as a circular cross section for the jet, and the position of the centerline is not affected by the small perturbations. Their boundary conditions included the jump in the pressure magnitude (5) and kinematic boundary condition on the surface. In the present study, only the stable electro-spinning region has been investigated. Hence, time-dependent terms could be eliminated and the governing perturbation equations for the electro-hydrodynamic behavior of the axisymmetric jet would be as follows, with known electric field components:

$$\bar{u}\bar{u}_x = -\bar{p}_x + \frac{1}{Re} 2\bar{u}_{xx} + \frac{6\bar{R}\bar{u}_x}{\bar{R}} \bar{u}_x + \beta \frac{2(1-\epsilon_p\sigma_{oi})}{\bar{R}} \bar{E}_{on} \bar{E}_r + \frac{1}{Fr} \bar{u} \bar{R}^2 \bar{u}_x = 0. \quad (6)$$

$$\frac{\bar{u} \bar{R}^2 \bar{u}_x}{2\bar{R}} = 0. \quad (7)$$

In Eq.(6), which is the momentum equation along the jet axis,  $oi$  and  $io$  indices represent the quantitative ratio of the exterior to interior fluid and vice versa, respectively. Equation(7) was obtained based on the kinematic boundary condition. From this equation, it has been observed that  $\bar{u} \bar{R}^2$  is constant and by using boundary condition  $\bar{R}(0) = \bar{u}(0) = 1$  at the nozzle tip, the axial velocity will be obtained as  $\bar{u} = 1/\bar{R}^2$ . In Eq.(6), the pressure which is composed of hydrodynamic and electrostatic pressure components can be calculated by the following equation:

$$\bar{p} = \frac{1}{We\bar{R}} - \frac{\bar{u}_x}{Re} - \frac{\beta}{2} (1 - \epsilon_p\sigma^2) \bar{E}_{oi}^2 - (1 - \epsilon_p) \bar{E}_i^2. \quad (8)$$

Electrical phenomena are described by Maxwell's electromagnetic equations. However, in the absence of external magnetic field condition, if the characteristic time scale of magnetic phenomena ( $t_M$ ) is much smaller than the characteristic time scale of electric phenomena ( $t_c$ ), magnetic effects can be ignored completely and the electrostatic equations furnish an accurate approximation.<sup>25</sup> Moreover, charges in the leaky dielectric fluid only accumulate at the interface, which can be considered as boundary effects and modifies the external electric field.<sup>25,26</sup> Therefore, for a leaky dielectric fluid system, the governing equation is reduced to simple electric current continuity law and can be represented as follows:

$$\nabla \cdot (\sigma \mathbf{E}) = 0, \quad (9)$$

where  $\sigma$  is the electric conductivity of the fluid. From the irrotational property of the electric field, it can be considered as the gradient of an electric potential  $\mathbf{E} = \nabla \Psi$  and we have

$$\nabla \cdot (\sigma \nabla \Psi) = 0. \quad (10)$$

It is assumed that due to the low electric conductivity of fluids, there is no charge transport at the electrode surfaces and, therefore, electric charges are only generated at the fluid-fluid interface and the net electric current is zero. To complete the description, a charge conservation equation is required at the

interface. By ignoring the charge diffusion mechanism, this equation can be written as<sup>25</sup>

$$\frac{c}{t_P} \frac{\partial q^s}{\partial t} + \frac{c}{t_F} \mathbf{u} \cdot \nabla_s q^s - q^s \mathbf{n} \cdot (\mathbf{n} \cdot \nabla) \mathbf{u} = -\sigma \mathbf{E} \cdot \mathbf{n}, \quad (11)$$

where  $t_c$  is the electrostatic time scale identified by the ratio of the dielectric permeability and conductivity,  $t_P$  is the transport process time rise from viscose relaxation and diffusion,  $t_F$  is the convective flow time which can be defined as the ratio of the flow length scale to the flow characteristics speed, and  $\nabla_s$  is the surface gradient. In this equation, the first term on the left represents charge relaxation, the second describes charge convection at the interface, and the third denotes changes in concentration due to dilation of the surface. Also, the term on the right stands for the charge transport to the surface by electro-migration. For a steady flow motion and assumption of instantaneous migration of charges to the interface,  $t_c/k_F \ll 1$ , Eq.(11) is reduced to the continuity of the electric current at the interface and is used as a boundary condition to solve the equation for the electric current equation.

In this study, the physical and electrical properties of the fluids are constant. Hence, the potential distribution (10) can be transformed into the potential Laplace equation which would be solved by the boundary integral approach as similarly used by Lac and Homsy.<sup>24</sup> They stated that the extent of the electric field on the surface is the average of interior and exterior electric fields in the vicinity of the interface. By applying the boundary condition of electric current continuity across the interface, i.e.,  $\sigma \mathbf{E} \cdot \mathbf{n} = 0$ , as well as applying the external electric field with the assumption of no free charges on the surface, the dimensionless boundary integral equation of the electric field for each of the surface elements can be obtained using the following equation:

$$\frac{\bar{E}_o + \bar{E}_i}{2} \Big|_p = \frac{\bar{E}_\infty}{E_0} + \frac{1 - \sigma_{oi}}{4\pi} \int_{(\bar{S})_q} \frac{(\bar{r})_{pq}}{(\bar{r})_{pq}^3} \bar{E}_{on} \cdot \bar{d}\bar{S}_q, \quad (12)$$

where  $p$ ,  $q$ , and  $(\bar{r})_{pq}$  are the field point, source point, and distance between these two points,  $\bar{E}_\infty$  is the applied electric field vector, and  $\bar{S}$  is the fluid-fluid interface, respectively. The first term on the right side of this equation represents the applied electric field at each point of the computational domain, and the second term represents the electric field correction at each point due to the existence of the potential surface. This equation includes two variables of  $\bar{E}_p$ , electric field vector at each point, and  $\bar{E}_{on}$ , electric field normal to the surface. Lac and Homsy<sup>24</sup> primarily solved this equation for each point of the surface which was obtained by the dot product of both sides of this equation by the unit normal vector of the field point ( $p$ ). Using this approach, the electric field normal to the surface in each point can be obtained as in the following equation:

$$\frac{1 + \sigma_{oi}}{2} \bar{E}_{on} \Big|_p = \frac{\bar{E}_\infty \cdot (\mathbf{n})_p}{E_0} + \frac{1 - \sigma_{oi}}{4\pi} \int_{(\bar{S})_q} \frac{(\bar{r})_{pq} \cdot (\mathbf{n})_p}{(\bar{r})_{pq}^3} \bar{E}_{on} \cdot \bar{d}\bar{S}_q. \quad (13)$$

After the calculation of the normal component of the electric field and its substitution into Eq.(12), the electric field vector

will be obtained for surface points. Thereafter, the tangential component of the electric field can be obtained with a vector subtraction, as in the following equation:

$$\vec{E}_t = \frac{\vec{E}_o + \vec{E}_i}{2} - \vec{E}_n \quad (14)$$

Since the tangential electric field component continues across the interface,  $\vec{E}_o = \vec{E}_i = \vec{E}_t$ .

### III. NUMERICAL SOLUTION

In the present study, the interface behavior of the liquid jet surrounded by air under uniform external electric field is analyzed. In order to numerically solve the boundary integral equation (13), the boundary element method was implemented. This numerical method required the initial surface for performing the calculations. Hence, it was primarily assumed that the electric field does not exist and the liquid jet leaves the nozzle with the radius of  $a$  with a determined flow rate of nozzle with the radius of  $a$  with a determined flow rate of  $Q = U\pi a^2$  under the gravitational force. In this condition, the initial surface was obtained; subsequently, applying the electric field will provide the actual, final jet profile.

Given the axisymmetric geometry of the electrified jet toward the central axis, the boundary integral equation can be solved on a line ( $\Gamma$ ); however, this equation has been obtained for a 3D surface. Therefore, the integral in Eq. (13), which is obtained on the fluid-fluid interface, is converting to double integrals in the azimuthal and axial directions that are given by Eq. (15). By the assumption of circular cross section for the jet,  $\vec{R}_q$  as well as  $\vec{E}_{o_n}$  are constant in the azimuthal direction of the following equation:

$$\vec{I} = \int_{(\Gamma)_q} \int_{(\tilde{S})_q} \frac{(\vec{r})_{pq} \vec{E}_i(\vec{n})_p}{(\tilde{r})_{pq}^3} \cdot \vec{n}_p \cdot \vec{E}_{o_n} \cdot \vec{R}_q d(\theta)_q d\tilde{r}_{pq} \quad (15)$$

Afterwards, the integrals in the azimuthal and axial directions can be solved using an analytical method and a numerical integral of the modified Gaussian point, respectively. The considered coordinate system for the electric problem is the right-handed and orthogonal coordinate, with the origin on the jet axis at the nozzle outlet. Hence, the distance of each point on the surface of the jet to the origin can be calculated by the following equation:

$$\vec{r} = \tilde{X} \vec{e}_i + \tilde{R} \cos \theta \vec{e}_j + \tilde{R} \sin \theta \vec{e}_k \quad (16)$$

In order to solve the boundary integral equation in the form of axisymmetric, the azimuthal integral of Eq. (15) should be solved,

$$\vec{I} = \int_0^{2\pi} \frac{(\vec{r})_{pq}}{(\tilde{r})_{pq}^3} d(\theta)_q \quad (17)$$

The integral of Eq. (17) is a vector integral with three components and can be defined as  $\vec{I} = \vec{I} / a$ . Following the analytical

following equation:

$$\begin{aligned} I_X &= \frac{4}{(A+B)^{3/2}} (\tilde{X})_p - (\tilde{X})_q \Pi \sqrt{m^2}, m \\ I_Y &= \frac{4}{(A+B)^{3/2}} (\tilde{R})_p + (\tilde{R})_q \left[ 1 - \frac{2}{m^2} \Pi \sqrt{m^2}, m \right. \\ &\quad \left. + (\tilde{R})_q \frac{2}{m^2} K(m) \right], \\ I_Z &= 0, \end{aligned} \quad (18)$$

where  $\Pi$  and  $K$  are the first and third kinds of complete elliptic integrals that can be accurately estimated by convergent series. The constant value of  $A$  and  $B$  and the integral module of  $m$  are defined as follows:

$$\begin{aligned} A &= (\tilde{X})_p - (\tilde{X})_q^2 + (\tilde{R})_p^2 + (\tilde{R})_q^2, \\ B &= 2(\tilde{R})_p(\tilde{R})_q, \\ m &= \frac{4B}{A+B} \end{aligned} \quad (19)$$

In case the source and field points are located on the symmetry axis, components of vector integral  $\vec{I}$  should be modified as in the following equation:

$$\begin{aligned} I_X &= \frac{2\pi}{(A+B)^{3/2}} \tilde{X}_p - \tilde{X}_q, \\ I_Y &= \frac{2\pi}{(A+B)^{3/2}} \tilde{R}_p. \end{aligned} \quad (20)$$

In this study, the axis of symmetry is aligned with the direction of  $\vec{E}_\infty = E_\infty \vec{e}_i$ . The initial interface profile is divided into  $N$  equal elements defining  $N + 1$  nodes which are located from the nozzle tip to the end of the jet where it is assumed truncated; therefore, there are no nodes that lie on the symmetry axis. The linear element is defined by two nodes at both ends and a node at the center of an element which is defined as the calculated node, and Gaussian points are distributed around this node for estimating the axial integral of Eq. (13). Similar to all previous studies in electro-spinning, only a certain

length of the jet is analyzed and the end of the jet is truncated. Hence, the simulated length should be long enough to avoid the occurrence of any numerical errors. Moreover, increasing the node number leads to a larger system of equations. Since the coefficient matrix resulted from the discretization process through the boundary element method is full, increasing the grid nodes affects the expense and accuracy of the computation. Therefore, in order to this problem, a tradeoff should be accomplished between the optimum number of grid and the required accuracy. Therefore, the grid size of 0.025 is used for the simulations.

According to the fluid electrical conductivity range that is used in the current study,  $\sigma_{oi}$  tends to zero and the effect of this parameter in governing equations (6), (8), and (12) will be neglected. Therefore, the terms including  $\sigma_{oi}$  have been

eliminated from governing equations for the simulations. Since the second fluid which has surrounded the jet is air,  $\epsilon_{io} = \epsilon_i$  in solution of the vector integral, the components of this integral which are  $\vec{I} = I_X \vec{e}_i + I_Y \vec{e}_j + I_Z \vec{e}_k$  can be obtained by the

this study.

After the calculation of normal and tangential components of the electric field using the boundary element method, the nonlinear equation (6) can be solved using the Newton

method. In this equation, the derivatives are discretized using the second-order central finite difference and the conditions of the jet downstream can be obtained by a second order extrapolation of last internal points of the grid.

## IV. RESULTS AND DISCUSSION

### A. Validation

#### 1. Simulation and comparison with literature

In this section, the suggested numerical method for the electro-spinning process will be validated by comparison between the simulation results and numerical and experimental results reported by Hohman *et al.*<sup>6</sup> Numerical and experimental results of Hohman *et al.*<sup>6</sup> for electro-spinning of glycerol were obtained using the parameters of Table III for different flow rates and potential differences. Dimensionless numbers of the present study due to physical parameters of Table III were represented in Table IV.

As it can be seen in Fig. 1, good agreement exists between the results of the present study and numerical results of the literature. Furthermore, there is very good agreement between our numerical results and experimental results for a flow rate-potential difference of 1-26, 1-30, and 1.5-30; however, differences can be noticed for other cases. In spite of considering the charge conservation equation consisting of electric charge convection and conduction terms, Hohman *et al.*<sup>6</sup> attributed the lack of agreement between their numerical and experimental results due to the inappropriate model for convection of the electric charges near the nozzle.

The electric charges entirely transport due to the conduction near the nozzle where the electric field is very large. In fact, low flow rates and high electric field justify the ignorance of charge transport by other mechanisms and the assumption of a static model for charges in this study. It can be seen from Fig. 1, with the constant flow rate, increasing the potential difference enhances the agreement between numerical and experimental results. In addition, comparing the numerical results indicated the lower contribution of the convection mechanism in the transport of electric charges at low flow rates.

TABLE III. Physical parameters of the glycerol fluid used by Hohman *et al.*<sup>6</sup>

$\rho$ $\frac{\text{kg}}{\text{m}^3}$	$\nu$ $\frac{\text{cm}^2}{\text{s}}$	$\gamma$ $\frac{\text{mN}}{\text{m}}$	$\epsilon$	$\sigma$ $\frac{\mu\text{S}}{\text{m}}$	$a$ (mm)	$d$ (cm)
1261	14.9	64	42.5	1	0.794	6

TABLE IV. Dimensionless numbers used for numerical simulation of an electrified jet in Fig. 1 based on the parameters in Table III, different flow rates (ml/min), and potential differences (kV).

	$\beta$			$We \times 10^3$	$Re \times 10^3$	$Fr \times 10^2$
	22 (kV)	26 (kV)	30 (kV)			
1.0 $\frac{\text{ml}}{\text{min}}$	13.3	18.6	24.8	1.1	4.5	0.9
1.5 $\frac{\text{ml}}{\text{min}}$	55.9	8.3	11.0	2.5	6.7	2.1
2.0 $\frac{\text{ml}}{\text{min}}$	3.3	4.7	6.2	4.4	9.0	3.6

Given the diagram of glycerol fluid behavior by Shin *et al.*,<sup>7</sup> our numerical simulations for a flow rate-potential difference of 1-22, which lies in the Rayleigh instability region, cannot predict the jet behavior. The possible reason is the curvature of the estimated surface for the stable jet which is inversely proportional to the local radius of the jet, i.e.,  $1/\bar{R}$ . In the numerical model by Refs. 5 and 6, the surface curvature was estimated as a combination of the local jet radius and its second derivative along the jet axis, i.e.,  $1/\bar{R} + 1/\bar{R}_{xx}$ , and the second derivative provided the feasibility of predicting the instabilities. Therefore, in order to predict the jet behavior in the aforementioned flow rate and potential difference, the surface curvature should be modified. Accordingly, the surface curvature in the present study was also modified as follows:

$$K = \frac{1}{R(1 + R_x^2)^{1/2}} - \frac{R_{xx}}{(1 + R_x^2)^{3/2}}, \quad (21)$$

which was proposed by Părău *et al.*<sup>28</sup> for predicting the instable bent jet behavior in the prilling process for evaluating the suggested surface curvature. The simulation result is represented in Fig. 1 after considering the modifications (i.e., 1-22). Estimation of the surface curvature using Eq. (21) is also capable for predicting the jet behavior in regions with severe gradients due to the derivatives of the jet radius along the axis, i.e.,  $\bar{R}_x$  and  $\bar{R}_{xx}$ .

#### 2. Simulation and comparison with experiment

The numerical model of Hohman *et al.*<sup>6</sup> was not primarily capable of predicting the jet behavior by applying a uniform external electric field. Moreover, they figured out that the protrusion length of the nozzle through the capacitor plate has a noticeable effect on non-uniformity of the electric field in the vicinity of the nozzle. To explain this discrepancy, they propounded the existence of the fringe field near the nozzle tip. When they included the effects of the fringe fields near the nozzle by simulating the experimental nozzle as a perfectly conducting solid cylinder and computed the electric field in the vicinity of the nozzle with the finite element method, agreement improved markedly between experimental observation and numerical computation. However, the numerical results of the present study (Fig. 1) approve that electro-hydrodynamic equations due to the application of uniform external electric field can correctly predict the jet behavior and there is no need to modify the external electric field near the nozzle tip.

The occurrence of this paradox was adequately persuasive for us to investigate experimentally the uneven behavior of the electric field near the nozzle. Accordingly, in the present study, certain experiments were prepared using the Newtonian fluid with properties listed in Table V and by different setups to induce the electric field near the nozzle.

To examine the initial jet development, the electro-spun jets close to the spinneret were photographed using a Canon EOS 6D DSLR camera, a 200 mm  $f/4d$  Micro Nikkor lens, and Canon 430 EXII speed light. The flow rate was adjusted by a TOP 5300 syringe pump through a metallic nozzle, and the electric field was formed by a high voltage power supply with a maximum nominal voltage of 30 kV and two aluminum

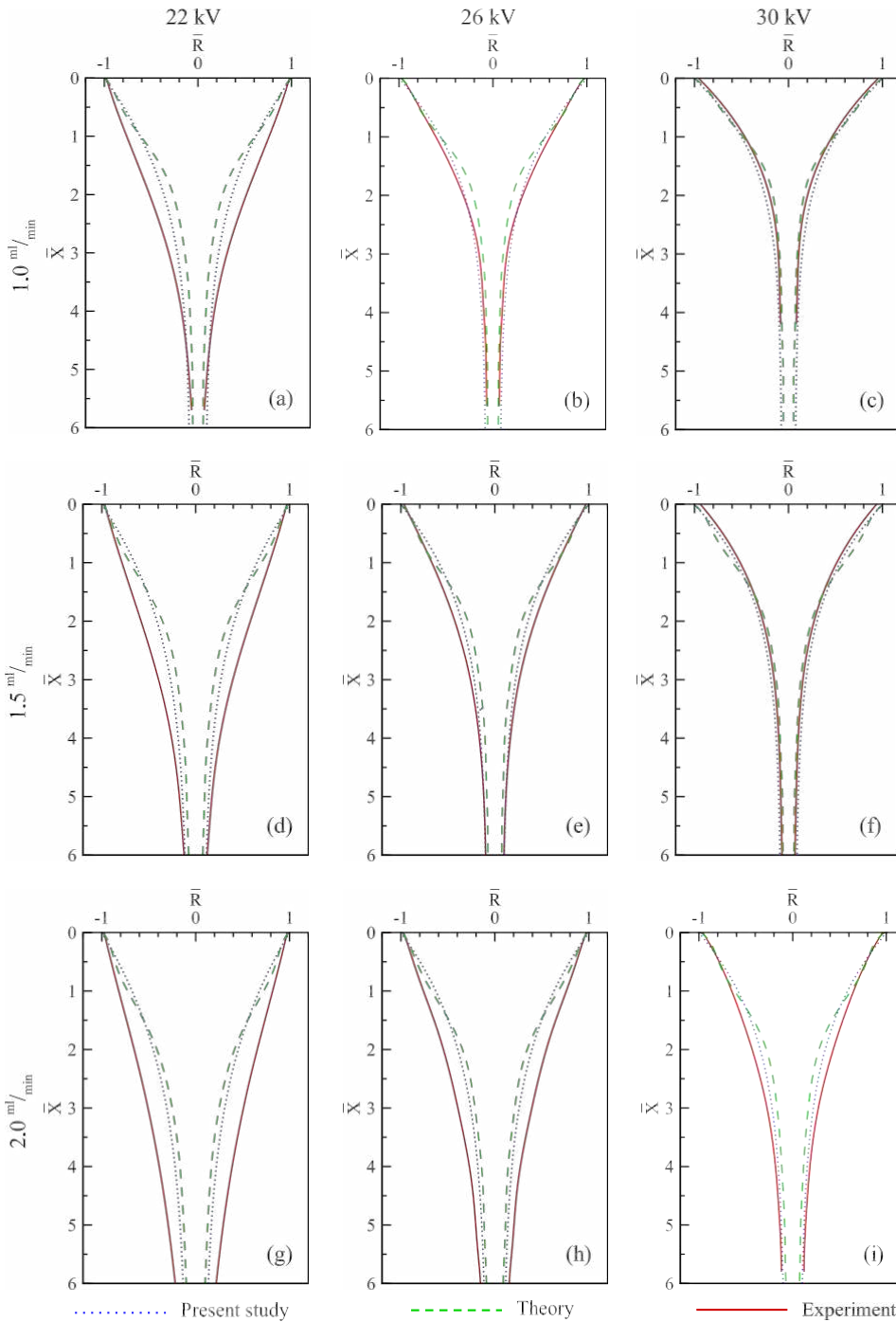


FIG. 1. Quantitative comparison of the numerical results of the present study (dotted line) with numerical results (dashed line) and experimental results (solid line) of Hohman *et al.*<sup>6</sup> for different flow rates and potential differences.

electrodes. Additionally, the solution viscosity, electrical conductivity, and surface tension were measured by a *DV II + Pro* viscometer, an *EU 3540* conductivity meter, *DCAT 11* surface tension, and *Libror AEU 210* balance measurement devices, respectively.

TABLE V. Properties of the utilized Newtonian fluid in 20°C.

$\rho$ $\frac{\text{kg}}{\text{m}^3}$	$\mu$ (Pa s)	$\gamma$ $\frac{\text{mN}}{\text{m}}$	$\epsilon$	$\sigma$ $\frac{\mu\text{S}}{\text{m}}$	$a$ (mm)	$Q$ $\frac{\text{ml}}{\text{min}}$	Collector dimensions $\text{cm}^2$
1273	1.18	63.23	40	0.26	0.35	0.026	8 × 8

The fluid jet leaves the metallic nozzle by applying an electric field during the electro-spinning process. By directly connecting one of the high voltage electrodes to the nozzle and the other one to the collector plate, the electro-spinning process will happen at a low potential difference in a far distance between the nozzle tip and the collector plate. However, as seen in Fig. 2 for this assembly of electrodes, the fluid jet will rapidly deviate from the straight line in the stable region. The cause of deviation could be the non-uniformity of the electric field in the vicinity of the nozzle. The point-plate assembly of electrodes was used by Carroll and Joo<sup>10</sup> in their numerical and experimental analyses. However, they did not mention details about how they calculated the



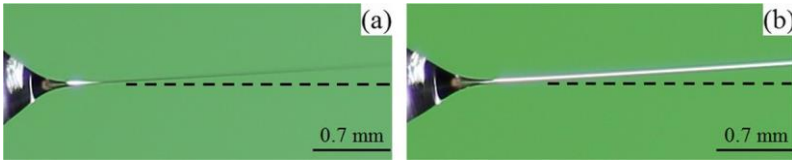


FIG. 2. Electro-spinning process with the connection of a high voltage source to the nozzle and demonstrating the deviation of the jet in the stable region from a straight line by applying a potential difference of 10 kV in a distance of 9 cm (a) and 15 cm (b) between the nozzle tip and the collector.

external electric field and the nature of  $E_\infty$  in their numerical simulations.

The protrusion of the metal nozzle from a metallic plate and connection of the high voltage source to this plate rather than the nozzle itself is another method to make the fluid jet leave the nozzle. As can be seen from Fig. 3, empirical studies show that the deviation of the fluid jet trajectory significantly reduced from the straight line in the stable region for the plate-plate configuration. However, it has been observed that by increasing the applied potential difference between the metal plate and the collector plate, the dimensions of the metal plate and the protrusion length of the nozzle are important factors on the jet deviation and elongation because the irregularity effects of the electric field near the nozzle were not entirely eliminated even though with the metal plate such that reducing the metal plate dimensions [Figs. 3(b) and 3(d)] or increasing the protrusion length of the nozzle [Figs. 3(a) and 3(f)] causes the jet deviation from the straight line and different elongation at a constant applied potential difference between the parallel plates. This mechanism was used by Hohman *et al.*<sup>6</sup> and Shin *et al.*<sup>7</sup> Hohman *et al.*<sup>6</sup> concluded that the protrusion length of the nozzle is an influential parameter in the stability of the fluid jet, but they did not express the effect of the metal plate dimensions on jet behavior.

Hartman *et al.*<sup>3</sup> used plate-plate as well as point-plate configurations for electro-spinning. The agreement between their numerical and experimental results indicates the validity of the numerical model in predicting the stable cone-jet mode. However, they did not explain the difference between these two mechanisms in electro-spinning, the calculation of the electric field in the vicinity of the nozzle, and the necessity of the numerical simulation of the nozzle.

It is obvious that for both methods, unevenness of the electric field near the nozzle causes the jet elongation as it leaves the nozzle. In fact, the difference between these two mechanisms is the relief of the electric field unevenness near the nozzle for

the plate-plate configuration. By comparing Figs. 2 and 3, it can be concluded that the metal plate attached to the nozzle has decreased the electric field irregularities as it has reduced the jet deviation from the straight line. Furthermore, increasing the stability of the jet is caused by increasing the uniformity of the electric field created by the plate-plate mechanism.

In our numerical model for electrified jet, we assumed that the position of the central axis of the jet is not affected by the small perturbations and the external electric field was uniform (12). Since it is necessary to provide experimental conditions in line with the numerical model to correctly compare these results, the experimental result of Fig. 3s shows that the plate-plate configuration with the nozzle protruding from a metal plate is better consistent with assumptions of the present simulation. Moreover, empirical studies showed that the electric field generated by a metallic capacitor plate of 8 cm, 8 cm and a nozzle protrusion length of 4 mm is closer to the numerical model assumptions [Figs. 3(b) and 3(e)].

In order to validate this proposition, a comparison was conducted between our numerical model results and experimental results. Figure 4 demonstrates this comparison of the experimental parameters of Table V and the corresponding dimensionless numbers used in numerical simulations, as listed in Table VI. As shown in the figure, the good agreement is achieved for the proposed electrode configuration.

In the numerical simulation, the surface curvature was defined based on Eq. (21) due to the severe gradients near the nozzle. Furthermore, a linear non-uniform mesh in which its mathematical equation follows a geometric progression with a coefficient of 4 (ratio of the last element grid size to the first one) was applied. This progression coefficient provides a dimensionless grid size of 0.025 near the nozzle. The number of nodes was 700, and the dimensionless length of the jet is also 35.

As it was previously mentioned in the section of the static electric charge model (Sec. IV A 1), numerical results of the

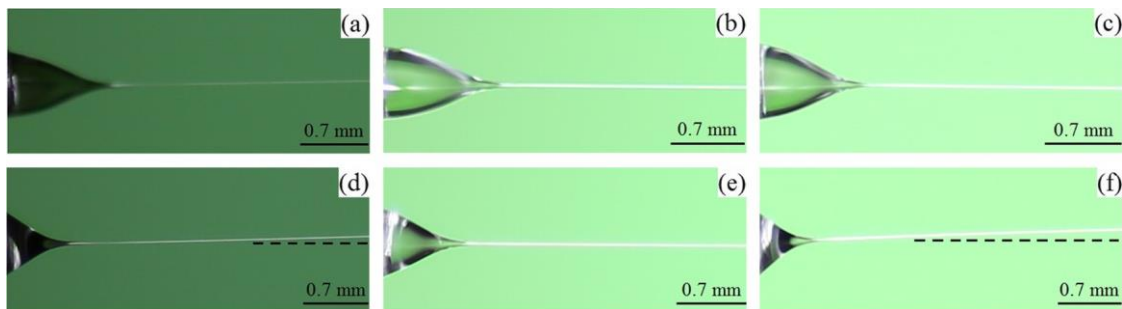


FIG. 3. Electro-spinning process with the protrusion of the nozzle from a metal plate and connection of the high voltage source to this plate in a constant distance of 5 cm between the parallel plates and different conditions of [metal plate dimensions (cm × cm), nozzle protrusion length (mm), applied potential differences (kV)]; (a) (2 × 2, 4, 20), (b) (8 × 8, 4, 23.5), (c) (8 × 8, 8, 17), (d) (2 × 2, 4, 23.5), (e) (8 × 8, 4, 25.5), (f) (8 × 8, 8, 20).

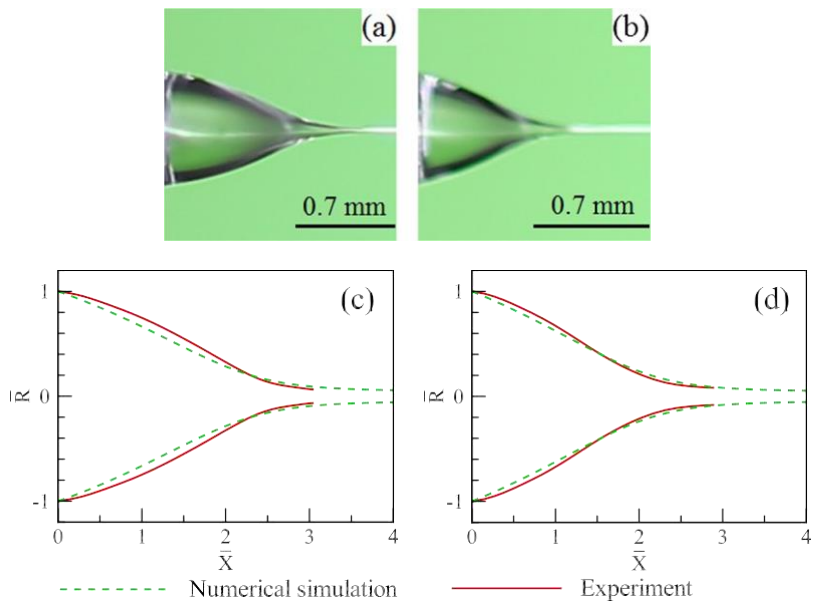
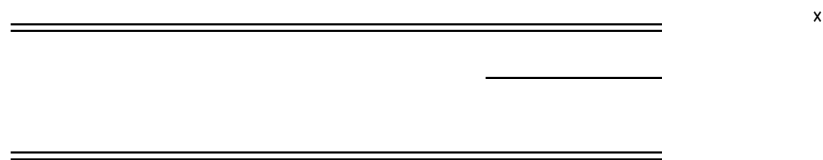


FIG. 4. Experimental images of glycerol jets for different conditions of (distance between parallel plates [cm], applied potential difference [kV]) (a): (3, 14); (b): (5, 24.5) and comparison of numerical results (dashed line) and experimental results (solid line) for different Beta dimensionless number ( $\beta \times 10^3$ ) (c): 1.19; (d): 1.31.



model is independent of the nozzle protrusion length and metal plate dimensions in predicting the behavior of the electrified jet under a uniform external electric field. To investigate how this geometry independence is feasible, the contour of the electric field component in the axial direction, i.e.,  $e_x$ , has been

zero at the nozzle (i.e.,  $\bar{X} = 0$ ). Moreover, it can be noticed that the local field will tend to the external electric field (i.e.,  $\bar{E}_x = 1$ ) at a farther distance from the nozzle.

The other important feature of an electrified jet is its asymptotic thinning behavior. Kirichenko *et al.*<sup>29</sup> and

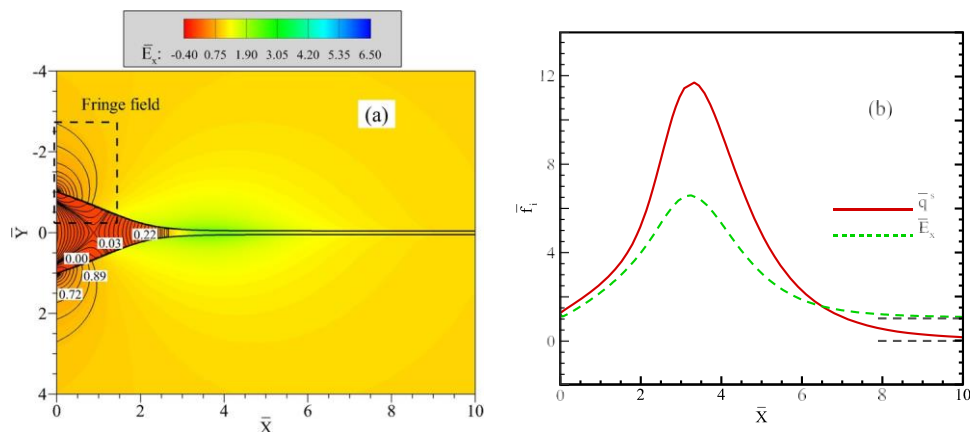


FIG. 5. Contour of the electric field component in the axial direction and formation of a fringe field near the nozzle tip using the boundary element numerical method (a) and changes of the electric charge and electric field axial component (b) along the jet.

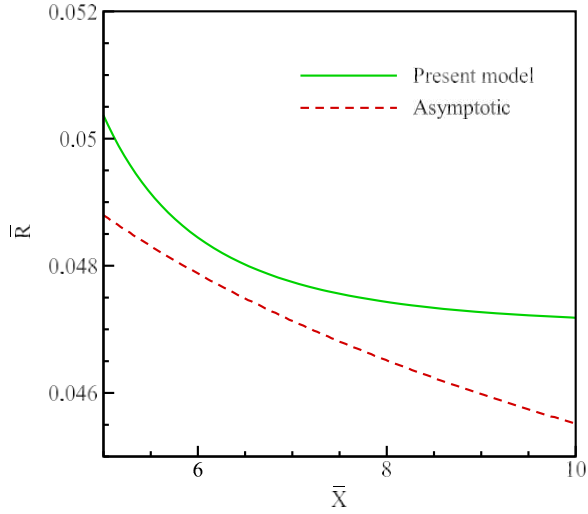


FIG. 6. The asymptotic behavior of the jet radius profile.

Ganon-Calvo<sup>30,31</sup> in their universal theory of electro-spraying first reported that the jet is thinned as  $\bar{X}^{-1/4}$  with the distance from the nozzle in an electric field. Later, Hohman *et al.*<sup>6</sup> reached to the same conclusion by making a balance between inertia, electric tangential stress, and gravity terms in the momentum equation. Since the electric term used in this study is different from Hohman *et al.*,<sup>6</sup> the proposed relation for the jet thinning asymptotic behavior should be modified by omitting the electric current term from the equation. Therefore, in our case, the jet is thinned only by the gravity force and we expect that the jet radius profile tends to  $X^{-4}$  with a coefficient proportional to  $Q^2$ . According to dimensionless

TABLE VII. Dimensionless numbers used in parameter study.

$We \times 10^4$	$\beta$	$Re \times 10^3$	$Fr \times 10^3$	$\sigma_{oi} \times 10^4$	$\epsilon_{io}$
5	40	2	5	1	30

numbers of Table VI with  $\beta = 1.31 \times 10^3$ , in Fig. 6, the jet radius profile is magnified for the region after the cone shape and a curve fit by  $\bar{X}^{-1/4}$  function obtained from the least square analysis is shown for the comparison.

### C. Parameter study

In order to analyze the effects of fluid physical properties, geometrical parameters, and flow characteristics on the behavior of the electrified jet, effects of various dimensionless numbers were studied. Table VII represents the main dimensionless numbers considered within the simulations. The effect of dimensionless numbers can be investigated by changing one of the numbers in a specific range while keeping others constant. The simulation results are illustrated in five distinct diagrams in Fig. 7 and will be discussed in more detail in the following.

The Coulomb repulsion between surface electric charges tends to form a conic geometry, while the surface tension of the fluid tends to maintain a spherical shape. Hence, by increasing the electric number ( $\beta$ ), the Coulomb repulsive force will overcome surface tension and the jet will be stretched in a short distance from the nozzle and tends to have a conic form [Fig. 7(a)]. It is also clear from the figure that a thinner jet is developed by increasing this number. Figure 7(b) shows

that by increasing the  $Re$  number the resistance force against

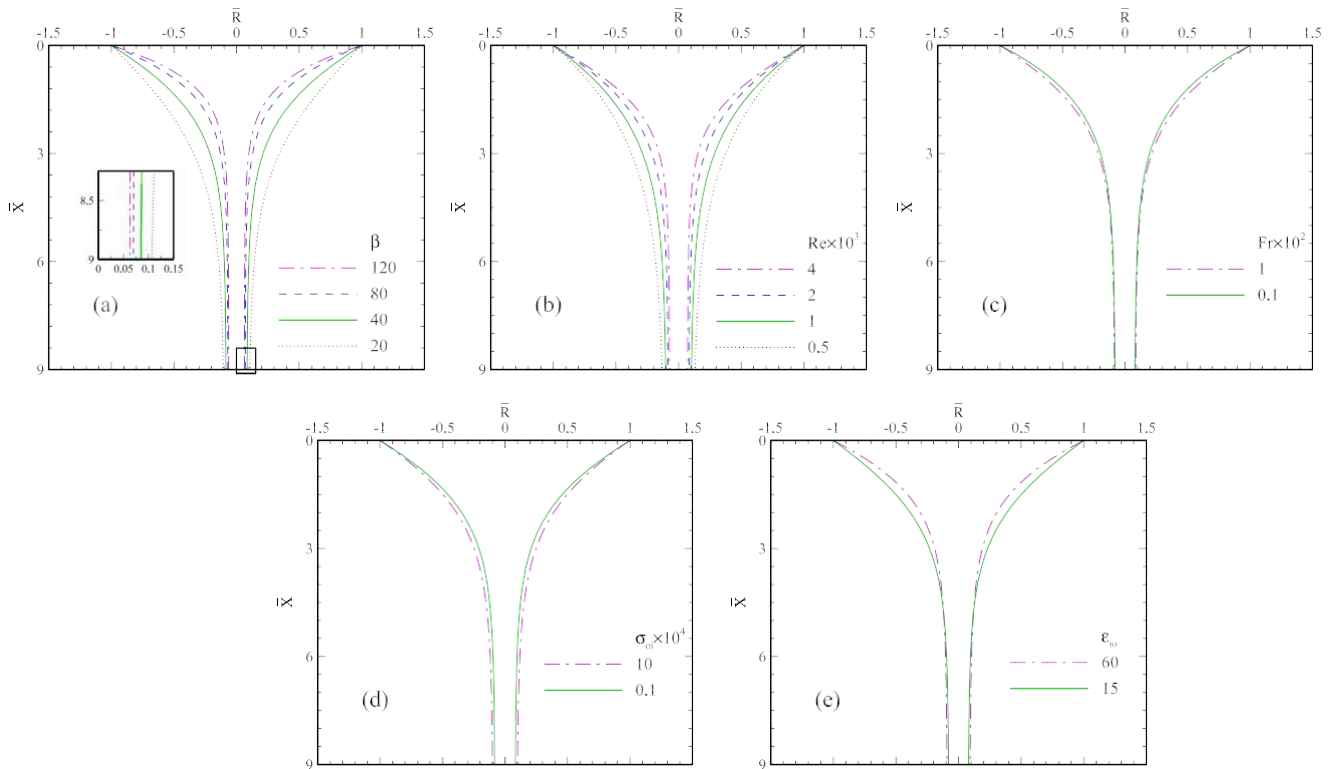


FIG. 7. Effects of dimensionless numbers  $\beta$  (a),  $Re$  (b),  $Fr$  (c),  $\sigma_{oi}$  (d), and  $\epsilon_{io}$  (e) on the changes of the electrified jet radius profile.

deformation decreases and the jet gets thinner, obviously. On the other hand due to the small flow rate, the bulk forces have a few effects on the jet behavior. Therefore, by decreasing the  $Fr$  number, there are no considerable changes on the jet profile, as shown by Fig. 7(c).

Decreasing the electric conductivity ratio means a higher conductivity of the fluid jet. As a result, the increased density of electric charges on the surface followed by the increased Coulomb repulsive force elongates the jet and makes it thinner. Since increasing fluid conductivity means that  $\sigma_{oi}$  tends to zero and the effect of this parameter in governing equations (6), (8), and (12) will be neglected, therefore, higher conductivity does not affect the radius profile change [Fig. 7(d)]. The electric permittivity coefficient of a fluid indicates the extent of electric energy stored in the fluid. In other words, it represents the ability of the fluid in polarization and creates normal stresses. By increasing the permittivity, the ability of polarization and consequently normal stresses to the surface increases which leads the jet to faster elongation due to the pressure decrease [Fig. 7(e)].

## V. CONCLUSION

In this study, a numerical model was suggested for predicting the behavior of a Newtonian leaky dielectric fluid in a uniform external electric field and stable cone-jet mode. The proposed model is independent of the nozzle geometry due to the boundary element numerical method applied for solving the governing electric equation. Electro-hydrodynamic equations include continuity, momentum, and electric Laplace equations, and contrary to previous studies, the charge conservation equation was not solved with the assumption of static electric charges which reduces the number of governing equations from 4 to 3. In order to validate the numerical model, a comparison was carried out between the numerical results of the present study and the numerical and experimental results of previous studies. This comparison indicated that in low flow rates and high potential difference, very good agreement exists between the results. The reason for the agreement can be attributed to the superior importance of conduction in electric charges rather than convection and changes of charge concentration due to surface dilation.

It is highly essential to consider experimental conditions in line with numerical formulations in order to conduct a correct comparison between the numerical and empirical results. Hence, several experiments were carried out to investigate different electro-spinning mechanisms, including the connection of the high voltage source to the nozzle or to a metal plate from which the nozzle is protruded. The difference between these two mechanisms is the reduction of electric field irregularities in the vicinity of the nozzle, followed by the deviation of the jet from a straight line. It was observed that in addition to the spinning distance (the distance between the nozzle tip or the attached metal plate to the nozzle and the collector plate), the dimensions of the metal plate attached to the nozzle and the protrusion length of the nozzle noticeably affect the electric field. Moreover, empirical results explain that the mechanism in line with the numerical formulation of the current study is

the connection of the high voltage source to the metal plate which is attached to the nozzle.

Analyzing the effect of dimensionless numbers on the jet behavior indicates that increasing  $\beta$ ,  $Re$ , and  $\epsilon_{io}$  numbers result in the formation of the stable cone-jet in a short distance from the nozzle. Additionally, increasing the dimensionless numbers of  $Fr$  and  $\sigma_{oi}$  primarily decreases the formation distance of the stable cone-jet from the nozzle.

- <sup>1</sup>A. Valipouri, A. A. Gharehaghaji, A. Alirezazadeh, and S. A. H. Ravandi, "Porosity characterization of biodegradable porous poly (L-lactic acid) electrospun nanofibers," *Mater. Res. Express* **4**(12), 125002 (2017).
- <sup>2</sup>J. J. Feng, "The stretching of an electrified non-Newtonian jet: A model for electrospinning," *Phys. Fluids* **14**, 3912–3926 (2002).
- <sup>3</sup>R. P. A. Hartman, D. J. Brunner, D. M. A. Camelot, J. C. M. Marijnissen, and B. Scarlett, "Electrohydrodynamic atomization in the cone-jet mode physical modeling of the liquid cone and jet," *J. Aerosol Sci.* **30**, 823–849 (1999).
- <sup>4</sup>A. F. Spivak, Y. A. Dzenis, and D. H. Reneker, "A model of steady state jet in the electrospinning process," *Mech. Res. Commun.* **27**, 37–42 (2000).
- <sup>5</sup>M. M. Hohman, M. Shin, G. Rutledge, and M. P. Brenner, "Electrospinning and electrically forced jets. I. Stability theory," *Phys. Fluids* **13**, 2201–2220 (2001).
- <sup>6</sup>M. M. Hohman, M. Shin, G. Rutledge, and M. P. Brenner, "Electrospinning and electrically forced jets. II. Applications," *Phys. Fluids* **13**, 2221–2236 (2001).
- <sup>7</sup>Y. M. Shin, M. M. Hohman, M. P. Brenner, and G. C. Rutledge, "Experimental characterization of electrospinning: The electrically forced jet and instabilities," *Polymer* **42**, 9955–9967 (2001).
- <sup>8</sup>J. J. Feng, "Stretching of a straight electrically charged viscoelastic jet," *J. Non-Newtonian Fluid Mech.* **116**(1), 55–70 (2003).
- <sup>9</sup>F. Yan, B. Farouk, and F. Ko, "Numerical modeling of an electrostatically driven liquid meniscus in the cone-jet mode," *J. Aerosol Sci.* **34**(1), 99–116 (2003).
- <sup>10</sup>C. P. Carroll and Y. L. Joo, "Electrospinning of viscoelastic Boger fluids: Modeling and experiments," *Phys. Fluids* **18**, 053102 (2006).
- <sup>11</sup>C. P. Carroll and Y. L. Joo, "Discretized modeling of electrically driven viscoelastic jets in the initial stage of electrospinning," *J. Appl. Phys.* **109**(9), 094315 (2011).
- <sup>12</sup>D. H. Reneker and A. L. Yarin, "Electrospinning jets and polymer nanofibers," *Polymer* **49**, 2387–2425 (2008).
- <sup>13</sup>F. J. Higuera, "Stationary coaxial electrified jet of a dielectric liquid surrounded by a conductive liquid," *Phys. Fluids* **19**(1), 012102 (2007).
- <sup>14</sup>F. J. Higuera, "Electrodispersion of a liquid of finite electrical conductivity in an immiscible dielectric liquid," *Phys. Fluids* **22**, 112107 (2010).
- <sup>15</sup>F. J. Higuera, "Electric current of an electrified jet issuing from a long metallic tube," *J. Fluid Mech.* **675**, 596–606 (2011).
- <sup>16</sup>C. P. Carroll, E. Zhmayev, V. Kalra, and Y. L. Joo, "Nanofibers from electrically driven viscoelastic jets: Modeling and experiments," *Korea-Aust. Rheol. J.* **20**(3), 153–164 (2008).
- <sup>17</sup>M. E. Helgeson, K. N. Grammatikos, J. M. Deitzel, and N. J. Wagner, "Theory and kinematic measurements of the mechanics of stable electrospun polymer jets," *Polymer* **49**(12), 2924–2936 (2008).
- <sup>18</sup>O. Karatay and M. Dogan, "Modelling of electrospinning process at various electric fields," *Micro Nano Lett.* **6**(10), 858–862 (2011).
- <sup>19</sup>X.-P. Tang, N. Si, L. Xu, and H.-Y. Liu, "Effect of flow rate on diameter of electrospun nanoporous fibers," *Therm. Sci.* **18**(5), 1447–1449 (2014).
- <sup>20</sup>O. Karatay, M. Dogan, T. Uyar, D. Cokeliler, and I. C. Kocum, "An alternative electrospinning approach with varying electric field for 2-D-aligned nanofibers," *IEEE Trans. Nanotechnol.* **13**(1), 101–108 (2014).
- <sup>21</sup>S. Ö. Gönen, M. E. Taygun, and S. Kükükbayrak, "Effects of electrospinning parameters on gelatin/poly (z-Caprolactone) nanofiber diameter," *Chem. Eng. Technol.* **38**(5), 844–850 (2015).
- <sup>22</sup>N. Ismail, F. J. Maksoud, N. Ghaddar, K. Ghali, and A. Tehrani-Bagha, "Simplified modeling of the electrospinning process from the stable jet region to the unstable region for predicting the final nanofiber diameter," *J. Appl. Polym. Sci.* **133**(43), 44112 (2016).
- <sup>23</sup>S. Raffei, B. Noroozi, L. Heltai, and A. K. Haghi, "An authenticated theoretical modeling of electrified fluid jet in core-shell nanofibers production," *J. Ind. Text.* **47**, 1791 (2017).

- <sup>24</sup>E. Lac and G. M. Homsy, "Axisymmetric deformation and stability of a viscous drop in a steady electric field," *J. Fluid Mech.* **590**, 239–264 (2007).
- <sup>25</sup>D. A. Saville, "Electrohydrodynamics: The Taylor-Melcher leaky dielectric model," *Annu. Rev. Fluid. Mech.* **29**, 27–64 (1997).
- <sup>26</sup>H. Paknemat, A. R. Pissevar, and P. Pourmaderi, "Numerical simulation of drop deformations and breakup modes caused by direct current electric fields," *Phys. Fluids* **24**, 102101 (2012).
- <sup>27</sup>M. Kang, R. P. Fedkiw, and X.-D. Liu, "A boundary condition capturing method for multiphase incompressible flow," *J. Sci. Comput.* **15**, 323–360 (2000).
- <sup>28</sup>E. I. Părău, S. P. Decent, M. J. H. Simmons, D. C. Y. Wong, and A. C. King, "Nonlinear viscous liquid jets from a rotating orifice," *J. Eng. Math.* **57**, 159–179 (2007).
- <sup>29</sup>V. Kirichenko, S. I. Petryanov, N. Suprun, and A. Shutov, "Asymptotic radius of a slightly conducting liquid jet in an electric field," *Sov. Phys. - Dokl.* **31**, 611–613 (1986).
- <sup>30</sup>A. M. Ganan-Calvo, "Cone-jet analytical extension of Taylor's electrostatic solution and the asymptotic universal scaling laws in electrospraying," *Phys. Rev. Lett* **79**, 217 (1997).
- <sup>31</sup>A. M. Ganan-Calvo, "On the theory of electrohydrodynamically driven capillary jets," *J. Fluid Mech.* **335**, 165–188 (1997).